Supporting information for

Response of a raft of particles to a local indentation

Wei He, Yiwei Sun, and Anthony D. Dinsmore*
Department of Physics, University of Massachusetts Amherst
**E-mail: dinsmore@physics.umass.edu*

Contents:

I. Shape of interface (theory)
II. $f(\delta)$, $df/d\delta$, and dimensionless plots for ordered rafts of various materials
III. $df/d\delta$ for two particle rafts with different sizes
IV. Forces and top-view images at different displacements
V. Displacements at the edge of the raft and the role of l_c
VI. $f(\delta)$ for disordered rafts
VII. Hysteresis in the $f(\delta)$ curve
VIII. Measured displacements

I. Shape of interface (theory)

The main text described measurements of the stiffness of particle-coated fluid interfaces. For comparison, we calculate here the $f(\delta)$ curves that should be obtained on fluid interfaces without particles. We call the resulting force $f_{\rm clean}$. The result of this derivation is Eqn. 1 of the main text.

First, we derive the capillary contribution to the force, f_c, following earlier work.[1] On a clean interface, the interfacial shape is determined by Young-Laplace equation,

$$\Delta p = 2\gamma H \quad \text{(S1)}$$

where H is the mean curvature and Δp is the pressure drop across the interface. Assuming that the system has no angle dependence and that the deformation is small ($|\nabla z| \ll 1$), and that Δp is from the weight of fluid above the interface, we have

$$\frac{1}{r}\frac{\partial}{\partial r}\left(r\frac{\partial z}{\partial r}\right) = \frac{z}{l_c^2} \quad \text{(S2)}$$

where $z(r)$ is the height of meniscus in cylindrical coordinates. This is the standard equation of capillarity in the small-slope regime. We further assume that the interface is infinitely large. These two assumptions naturally lead to the following boundary conditions

$$z(\infty) = 0 \quad \text{(S3)}$$

$$f_c = 2\pi R_c \gamma \frac{dz}{dr}|_{r=R_{\rm in}} \quad \text{(S4)}$$

where f_c is the capillary force and $R_{\rm in}$ is the radius of the indenter's rim. Combining Eqns. S2-S4, we have

$$z(r) = \frac{f_c}{2\pi\gamma \frac{R_c}{l_c}} \frac{K_0\left(\frac{r}{l_c}\right)}{K_1\left(\frac{R_{\rm in}}{l_c}\right)} \quad \text{(S5)}$$

where $K_n(x)$ is the modified Bessel function of second kind. Along with an extra condition

$$z(R_{\rm in}) = \delta \quad \text{(S5),}$$

and defining a rescaled indenter radius $\tilde{R} = \frac{R_{in}}{l_c}$, we have

$$f_{\mathrm{c}} = 2\pi\gamma\tilde{R}\frac{K_1(\tilde{R})}{K_0(\tilde{R})}\delta \quad \text{(S6)}$$

There is also a force (f_{h}) owing to the net weight of displaced fluids, which leads to a hydrostatic pressure. This force equals the weight of the fluid that is displaced under the contact ring,[2] which is $f_{\mathrm{h}} = \pi R_{\mathrm{in}}^2\delta(g\,\Delta\rho)$. In terms of dimensionless quantities, $f_{\mathrm{h}} = \pi\gamma\tilde{R}^2\delta$.

Finally, the total force acting on the indenter at a fluid-fluid interface is the sum of the capillary part f_{c} and the gravity component f_{h}. The result is

$$f_{\mathrm{clean}} = f_{\mathrm{c}} + f_{\mathrm{h}} = 2\pi\gamma\tilde{R}\frac{K_1(\tilde{R})}{K_0(\tilde{R})}\delta + \pi\gamma\tilde{R}^2\delta \quad \text{(S7)}$$

which is Eqn.(1) of the main text.

II. $f(\delta)$, $df/d\delta$, and dimensionless plots for ordered rafts of various materials

We measured $f(\delta)$ for many combinations of fluids and particles, as summarized in the main text. Here we provide some more of the data.

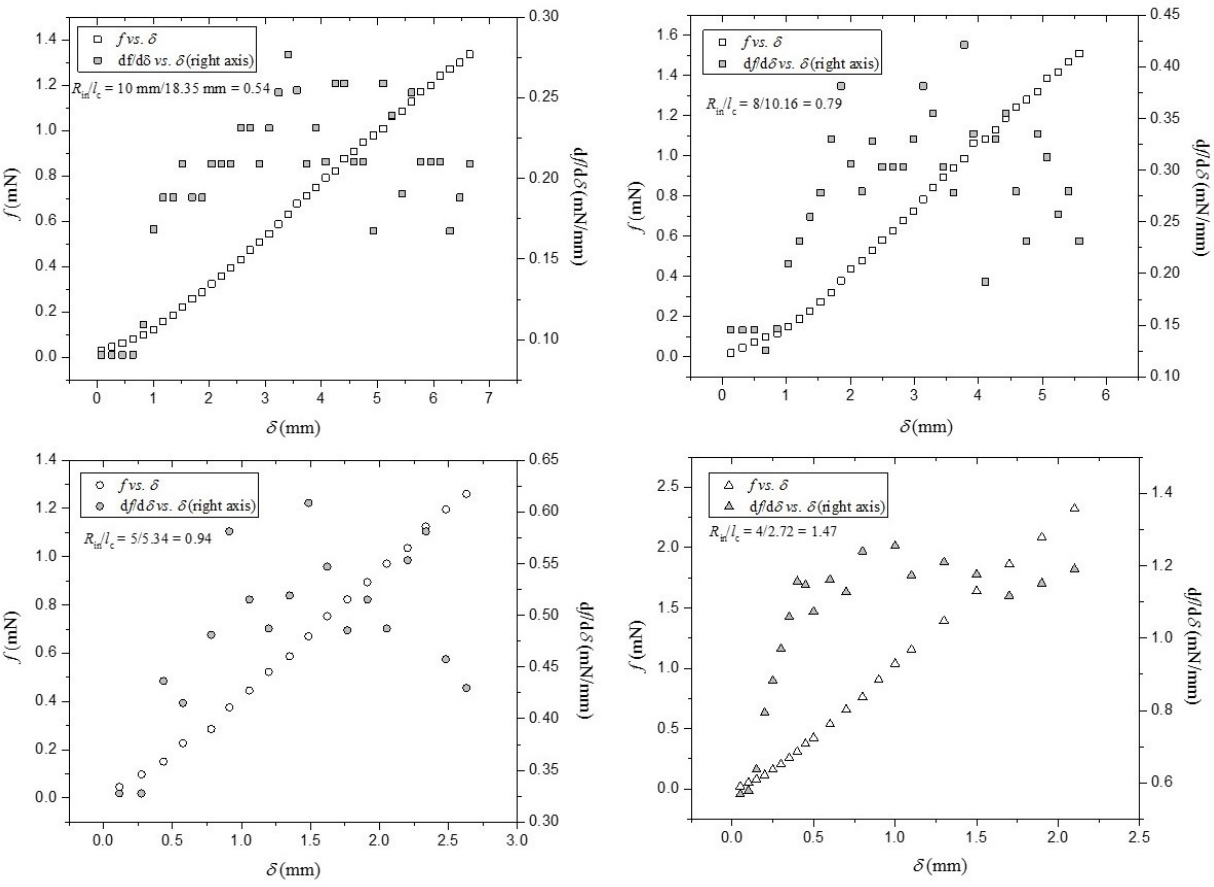

Supporting Fig. S1. Measured force, f (left axis) and stiffness (right axis) versus indentation, δ, for different combinations of particles, liquids and indenters. Each plot indicates the values of R_{in} and l_{c}.

To highlight the essential parameters, we show the data in rescaled, dimensionless form. We defined dimensionless parameters as follows:

$$\tilde{F} = \frac{f}{\left(\frac{df_{\text{clean}}}{d\tilde{\delta}}\right)} = \frac{K_0(\tilde{R})}{\pi\tilde{R}^2 K_0(\tilde{R}) + 2\pi\gamma\tilde{R}K_1(\tilde{R})}\frac{f}{\gamma l_c} \quad \text{(S8)}$$

where f and δ are the measured values, f_{clean} was defined in Eqn. (1), and $\tilde{\delta} = \delta/l_c$. In Fig. S2, we replotted the data of Fig. 2 after rescaling force and displacement according to Eqn. (S8). The regime $\tilde{\delta} < 0.2$ corresponds to the 1st plateau and the data did not scale. In the range $0.2 \lesssim \tilde{\delta} \lesssim 0.5$, we found consistent scaling (2nd plateau region). Beyond the second plateau region, the slope of $\tilde{F}(\tilde{\delta})$ decreased, contrary to Eqn. (2). We attribute this deviation to two causes. First, the small-slope approximation might not be accurate in this large-$\tilde{\delta}$ limit. Second, we noticed that particles next to the indenter rolled upward onto the indenter, which tended to raise the interface and reduce the interface slope and thus the capillary force. This trend did not scale with l_c, as is evident from the absence of data collapse in this regime.

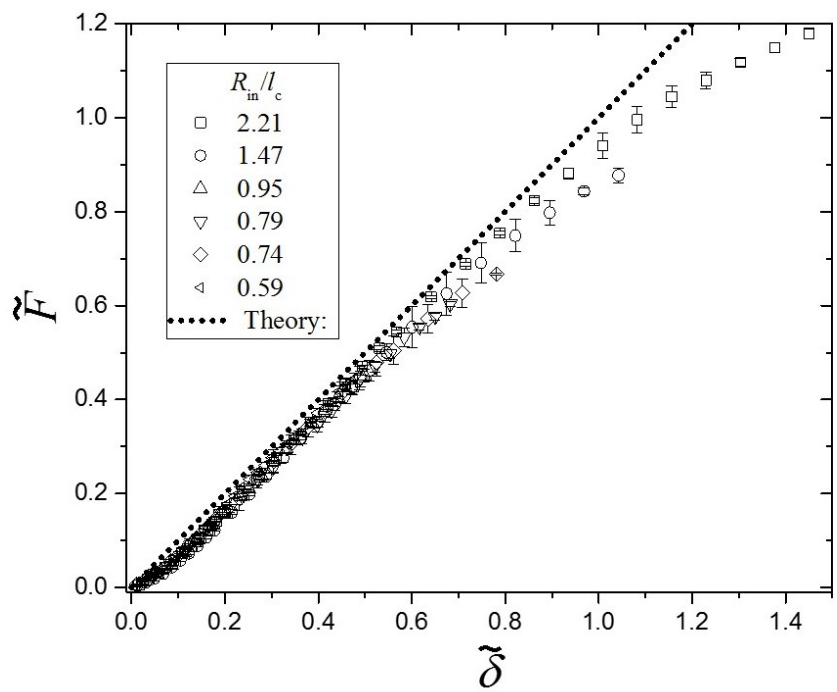

Supporting Fig. S2. Normalized force-indentation curves for the data shown in Fig. 2 of the main text. The dotted line is the theoretical calculation for a clean fluid interface, $\tilde{F} = \tilde{\delta}$.

III. $df/d\delta$ for two particle rafts with different sizes.

Figure S3 shows measurements of two rafts composed of Teflon particles at an air-water interface. One raft was the standard size (30-mm radius) and the other matched the size of the indenter. We could discern no difference between the two, indicating that the particles on the free fluid interface play a negligible role in the effective stiffness. The extent of the first plateau was quite small relative to other systems studied because of the small l_c.

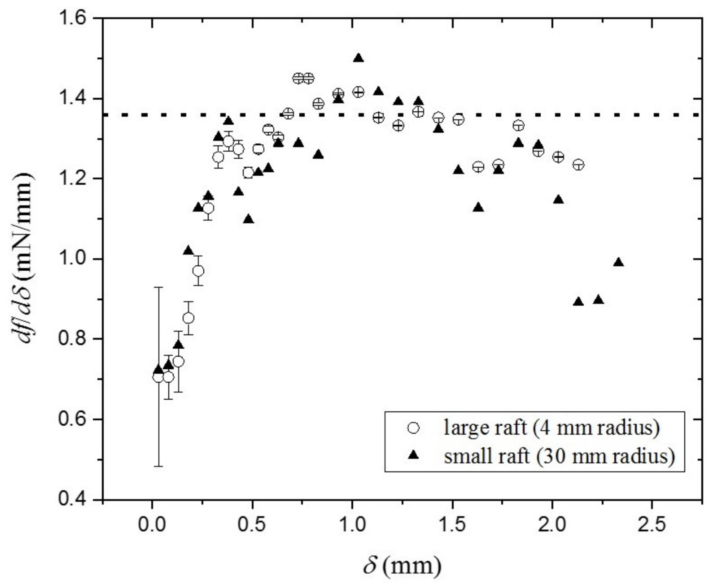

Supporting Fig. S3 Measured $df/d\delta$ *vs.* δ for two particle rafts with different sizes over the full range of δ. (Teflon particles at water-air interface). The small raft was similar in size to the indenter (R_{in} = 4 mm). The large raft was 30 mm in radius, the size used in most of the experiments reported here. The dotted line is the clean-interface result, from Eqn. (1).

IV. Forces and top-view images at different displacements

Figures S4-S6 show the results for a typical experiment, in which we pushed a 4 mm-radius circular, flat-bottom indenter through a raft at an air-water interface. The raft was composed of Teflon spheres with radius $a = 0.79 \pm 0.05$ mm. In Fig. S4, the open symbols show the measured $f(\delta)$ for this raft. The numbered data points correspond to the images and labels in Fig. S5. The filled symbols show the measured $f(\delta)$ curve measured for the bare air-water interface, prior to adding the Teflon particles onto the interface.

In Fig. S4, the experimental data for the clean interface agree closely with the theory for small δ, and then become slightly smaller than theory at larger δ. We attribute this deviation partly to a breakdown of the small-slope approximation in the theory, and partly to our observation that the contact line could not perfectly pin on the edge of the indenter. It would advance towards the center, and hence reduced the force.

Top-view images at selected instances are shown in Fig. S5. At the beginning (pictures 1 and 2), there was no noticeable in-plane movement of particles. As δ was increased, some of the particles displaced toward the indenter. As an example, at moment 5 it is clear that only particles in certain directions had moved toward the indenter. Such displacements are the origin of the star-shaped pattern developed in the raft. For clarity, this same image is reproduced at larger size in Fig. S6 (and also shown in Fig. 5*a* of the main text). As the indenter moved further downward, the raft was further stretched in the radial direction, as shown in moment 6. To demonstrate that the edge particles did not displace to a measurable extent, we have sketched the edge of the first image (in red) and overlaid it on the last image with only small rotation and translation to allow for raft movement.

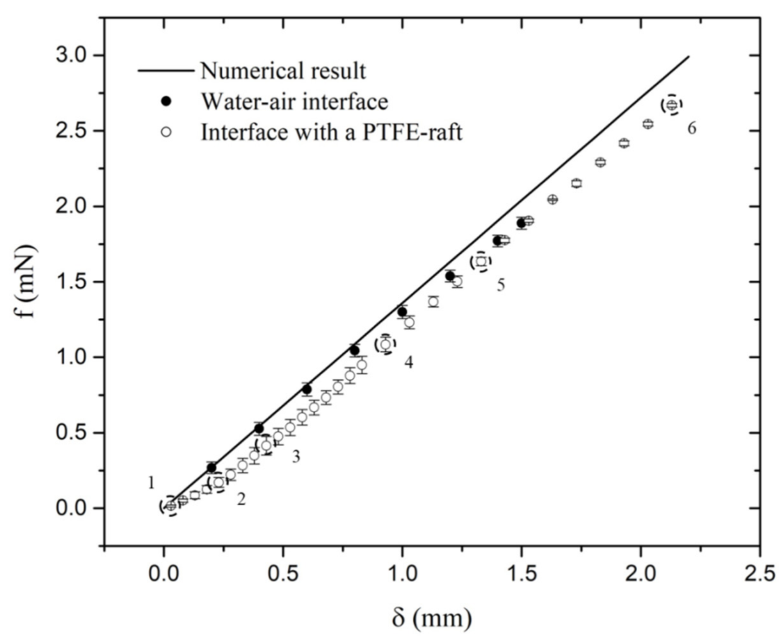

Supporting Fig. S4. Measured force, f *vs.* indentation, δ, for a 4-mm-radius circular bottom indenter. Data are for a clean interface (●) and for a raft-coated interface (○). The raft experiment is the same as for Figs. S5-S6 and the labels 1-6 around some of the data points correspond to the images of Fig. S5.

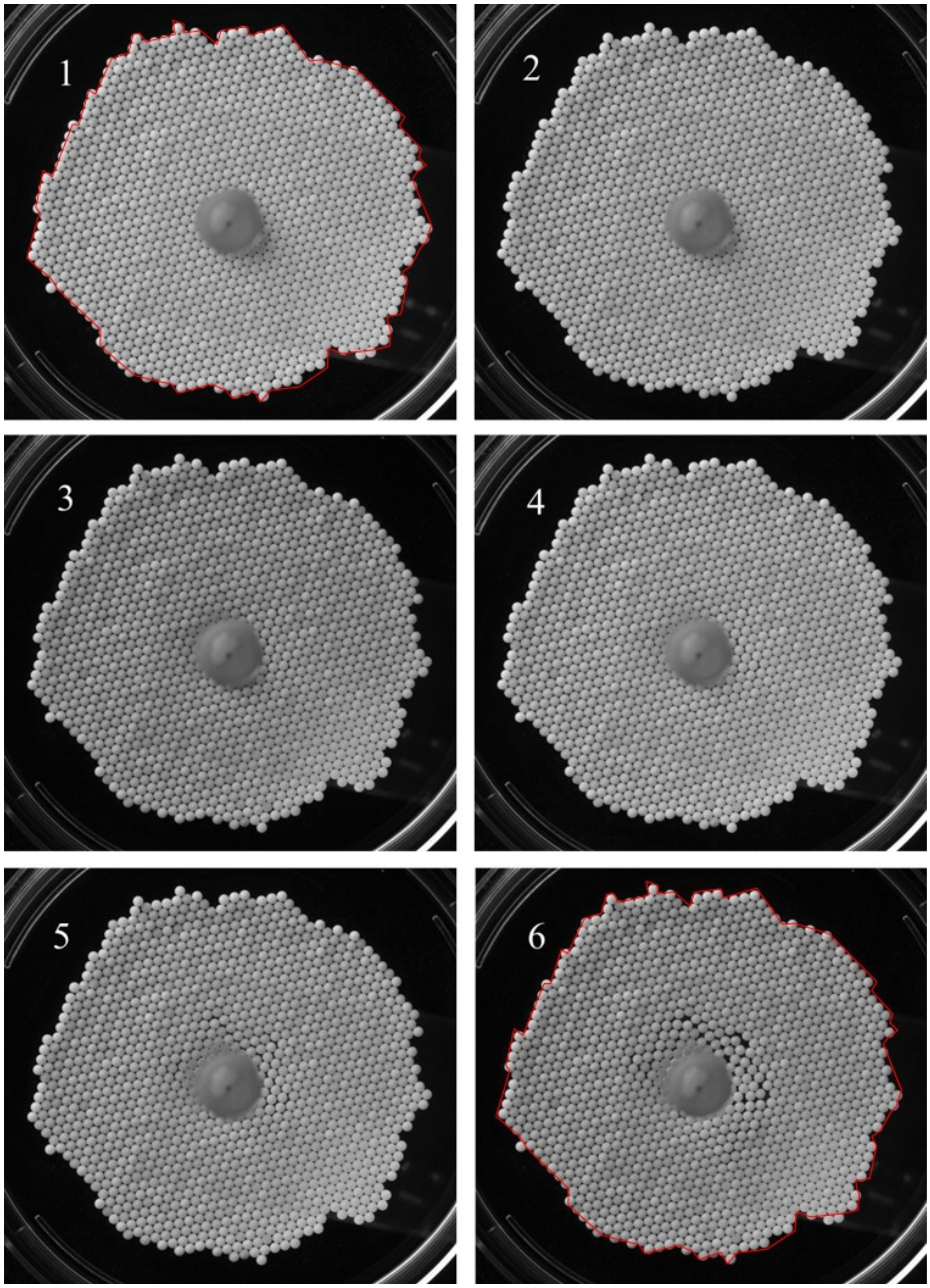

Supporting Fig. S5. Top-view images of the particle raft at various indentations. This raft is the same as in Fig. S4, composed of Teflon particles (a = 0.79 $\pm$ 0.05 mm) and R_{in} = 4 mm at a water-air interface. The first image shows the raft perimeter drawn in red. The last image shows that same shape from the first image, but slightly rotated to match the raft's position.

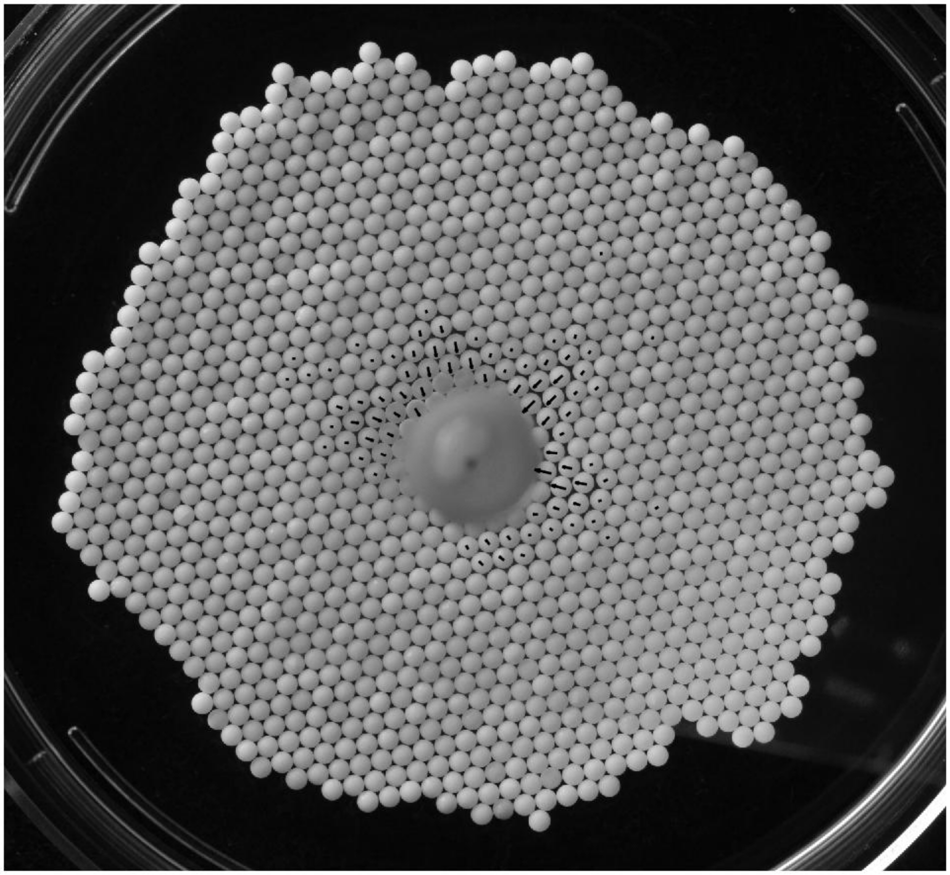

Supporting Fig. S6. Projected displacement field of Teflon particles at a water-air interface. This is the same image as #5 of Fig. S4 but with the arrows added to indicate displacements. Displacements were measured in the plane of the image and are shown magnified by 10×.

V. Displacements at the edge of the raft and the role of l_c

Figure S7 shows plots of the mean diameters of rafts of similar sizes at interfaces with different l_c. At the air-water interface (Fig. S7*a*), the raft diameter was approximately 20 l_c and it grew by about 0.2%, which may be experimental error. This is the same kind of raft as in Figs. S4-6 but with a different indenter and both showed negligible displacement at the raft's edge. At the oil-water interface (Fig. S7b), the initial raft diameter was 6.1 l_c and the size systematically shrank by 1% during the indentation. The particles at the edge moved inward.

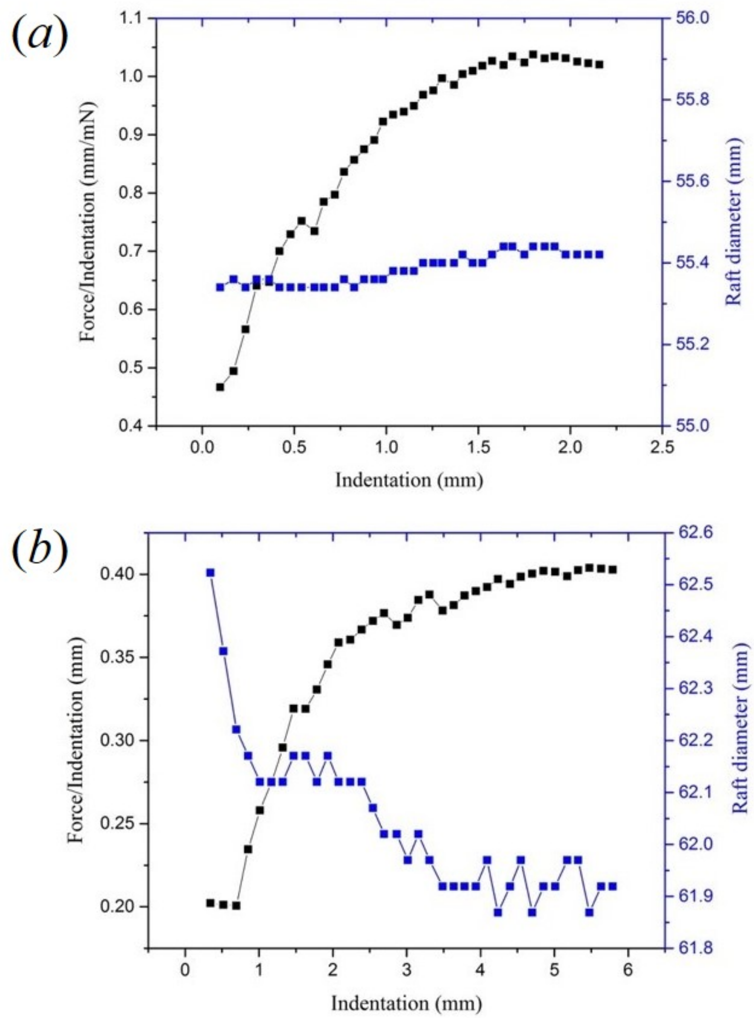

Supporting Fig. S7. Plots of measured f/δ (left axis, black symbols) *vs*. displacement δ. Also shown is the average diameter of the raft (right axis, blue symbols). (***a***) Teflon particles at a water-air interface with l_c = 2.72 mm and R_{in} = 3.43 mm. (***b***) PS particles at the interface between water and a mix of hexane and silicone oil, with l_c = 10.16 mm and R_{in} =10 mm.

VI. $f(\delta)$ for disordered rafts

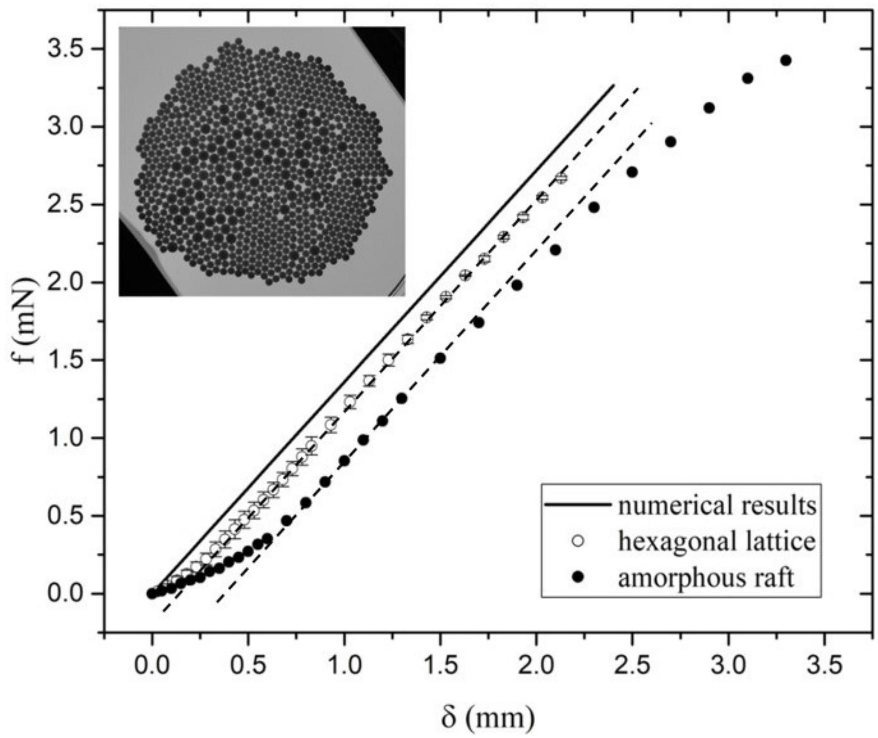

Supporting Fig. S8. Measured $f(\delta)$ for a hexagonally packed lattice (○) and an amorphous raft (●). The solid line shows the prediction of Eqn. (1). The two dashed lines are parallel to the solid line (*i.e.*, have the same stiffness) and are shown for comparison to the data. The inset is a top-view image of the amorphous raft at the start of the experiment. For both rafts (and especially the amorphous one), the stiffness falls off when $\delta \gtrsim 2$ mm. As described in the text, we attribute this to a change in the 3-phase contact line near the indenter. The first plateau was considerably extended in the amorphous raft, which we attribute to the presence of the larger particles in it.

VII. Hysteresis in the *f*(δ) curve.

Figure S9 shows a plot of force vs displacement for a water-air interface (l_c = 2.72 mm) with Teflon particles and R_{in} = 4 mm.

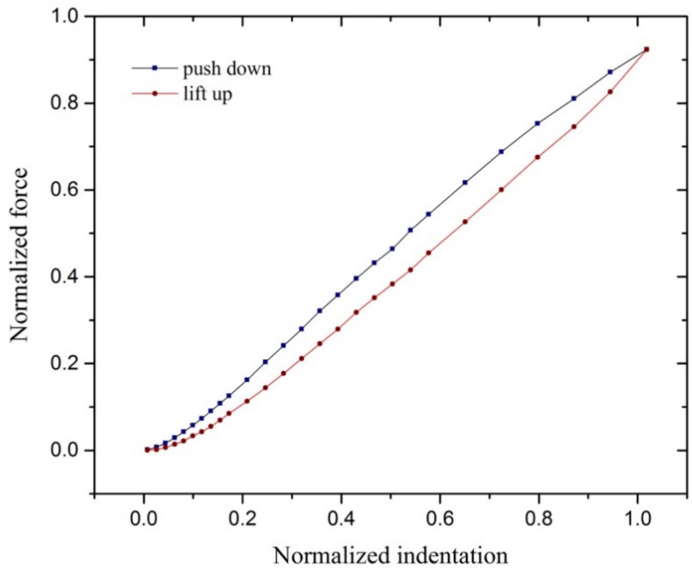

Supporting Fig. S9. Measured force vs displacement for a water-air interface (l_c = 2.72 mm) with Teflon particles and R_{in} = 4 m. The direction of indentation was reversed prior to the film rupture.

VIII. Measured displacements.

Figure S10 shows how the particles moved between the undeformed configuration (#1) and the indented configuration (#5) for the experiment of Figs. S4-6. By assuming that the particles remained on the interface, and furthermore that the interface shape was the same as for a clean fluid (Eqn. S5), we were able to calculate the correct Euclidean distance between particle centers. Figure S10(*b*) shows the inter-particle separations for one section of the raft. Initially (in configuration #1), the separations were approximately 2*a* (=1.59 mm), indicating that particles were close-packed as expected. After indentation, however, separations increased by up to 15% along the radial direction but remained approximately close-packed along the azimuthal (θ) direction. At radial distances (r) more than approximately 13 mm, we could discern no particle displacements relative to $\delta = 0$.

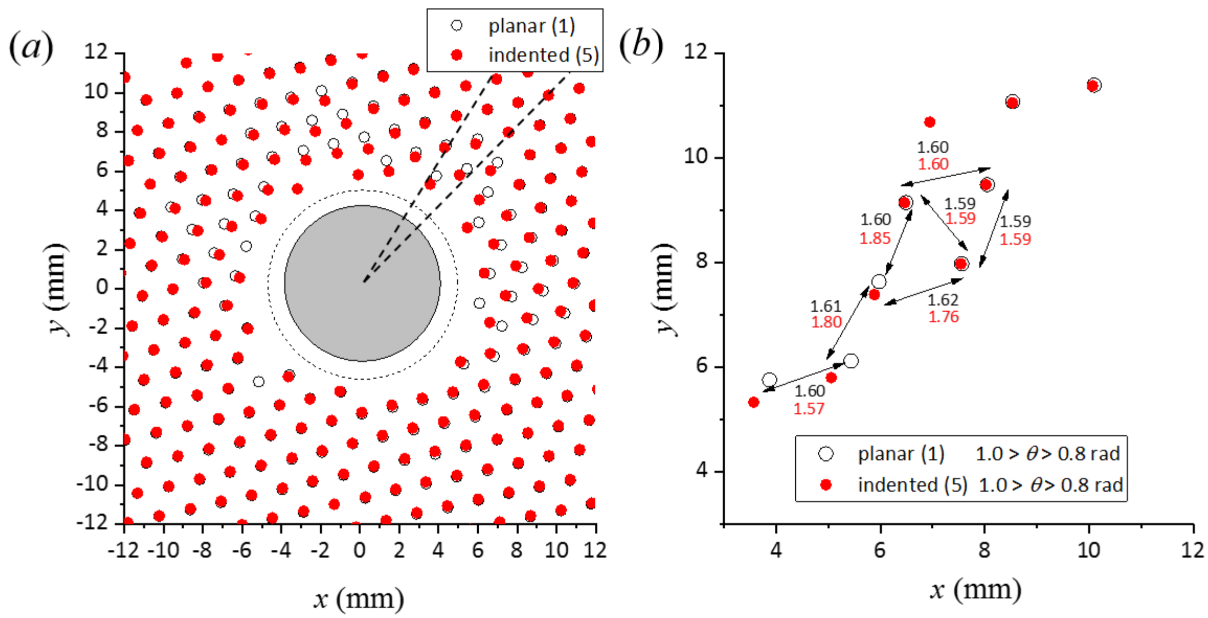

Supporting Fig. S10. Measured positions and displacements of particles from the configurations labeled #1 and #5 in Figs. S4-6. In each case, the particles in #1 are represented by open circles and in #5 by the red filled circles. Positions were extracted from camera images. (*a*) A top-down image. The indenter is represented by the gray disc and the dashed circle shows the closest approach of a particle's center of mass (radius $R_{in} + a$). Particles in contact with the indenter were typically not tracked because of image distortion. (*b*) The same data for those particles with angular positions, θ, between 0.8 and 1.0 radians, corresponding to the wedge shown by the dashed lines in (*a*). The separations between particles, in mm, are shown in black for configuration #1 and in red for configuration #5. The two innermost particles were the only ones separated by less than a particle diameter, but we attribute this to errors from tracking particles next to the indenter. The particles shown in this plot are the same as those shown in Fig. 5(*b*) of the main text.

References cited in the SI:

(1) Vella, D.; Mahadevan, L. *Am. J. Phys.* **2005**, *73*, 817.
(2) Keller, J. B. *Phys. Fluids* **1998**, *10*, 3009-3010.